Supporting Information

Comparative study of multicellular tumor spheroid formation methods and implications for drug screening

Maria F. Gencoglu[‡], Lauren E. Barney[‡], Christopher L. Hall[‡], Elizabeth A. Brooks[‡], Alyssa D. Schwartz[‡], Daniel C. Corbett[§], Kelly R. Stevens[§] and Shelly R. Peyton*[‡]

[‡]: Department of Chemical Engineering, University of Massachusetts Amherst, N540 Life Sciences Laboratories, 240 Thatcher Rd, Amherst, MA 01003-9364.

[§]: Department of Bioengineering, University of Washington, Box 355061, Seattle, WA, 98195-5061.

*Corresponding author: speyton@ecs.umass.edu

15 pages, 2 tables, 11 figures

Materials and Methods:

RGD synthesis

GRGDSPCG was synthesized on a CEM's Liberty Blue automated solid phase peptide synthesizer (CEM, Matthews, NC) using Fmoc protected amino acids (Peptide Solutions LLC, Las Vegas, NV). Resin was cleaved from the peptide by sparging nitrogen gas through a solution of peptide-resin and trifluoroacetic acid, triisopropylsilane, water, 2,2′-(Ethylenedioxy)diethanethiol at a ratio of 92.5:2.5:2.5:2.5 % by volume, respectively (Sigma-Aldrich, St. Louis, MO) for 3 hours at room temperature in a peptide synthesis vessel (ChemGlass, Vineland, NJ). The peptide solution was filtered to remove the cleaved resin, and the peptide was precipitated out using dimethyl ether at -80 °C (Thermo Fisher Scientific, Waltham, MA). Molecular mass was validated using a MicroFlex MALDI-TOF (Bruker, Billerica, MA) using α-cyano-4-hydroxycinnamic acid (Sigma-Aldrich, St. Louis, MO). Peptides were purified to ≥95% on a VYDAC reversed-phase c18 column attached to a Waters 2487 dual **λ** absorbance detector and 1525 binary HPLC pump (Waters, Milford, MA).

Gene Expression Clustering and PCA

RT-PCR data was clustered using a heatmap in R programming to generate dendrograms. Principal component analysis employed the “Using the devtools” package and “factoextra R” library to calculate principal components 1 and 2, and the shaded ovals representing 0.5 probability are shown in Figure 2b. Gene set enrichment analysis (GSEA) was performed on RNA collected from MDA-MB-231 and SkBr3 cells on TCPS, from polyNIPAAM and from cells grown in polyNIPAAM for 14 days before being dissociated to single cells back onto TCPS for 24 hours. A ranked list was generated from these samples, and enrichment of gene sets was analyzed. Normalized enrichment scores are reported from this analysis. The accession number for the RNA-Seq data is GSE93562.

Table S1: Characterization of gene expression by RT-PCR.

Gene	Accession #	Position	Forward sequence, 5'-3'	Position	Reverse sequence, 5'-3'
CLDN4	NM_001305.4	678	CAAGGCCAAGACCATGATCG	920	GAGTAAGGCTTGTCTGTGCG
CDH3	NM_001793.5	11	GGAGGTGGAGAAAGAGGCTT	223	ACTCCTCAGCCTCCTCAGTA
CDH5	NM_001795.4	1075	TACCAGGACGCTTTCACCAT	1298	AAAGGCTGCTGGAAAATGGG
ITGB4	NM_000213.3	2946	ACTACACCCTCACTGCAGAC	3154	TCTGGCTTGCTCCTTGATGA
ITGA2	NM_002203.3	1784	GGGCATTGAAAACACTCGAT	1966	TCGGATCCCAAGATTTTCTG
ITGB1	NM_002211.3	2054	CATCTGCGAGTGTGGTGTCT	2262	GGGGTAATTTGTCCCGACTT
FN1	NM_212482.2	391	CGGTGGCTGTCAGTCAAA	520	AATCCTCGGCTTCCTCCATAA
RPS-13	NM_001017.2	217	AAGTACGTTTTGTGACAGGCA	403	CGGTGAATCCGGCTCTCTATTAG
β-actin	NM_001101.3	747	GGACTTCGAGCAAGAGATGG	980	AGCACTGTGTTGGCGTACAG

Table S2: Pathology report of patient samples.

Patient	Age	Diagnosis	Treatment
P1		Malignant ascites	Cisplatin, and etoposide
P2		Ovarian cancer with omental metastasis	None
P3	76	Uterine cancer and ascites	Carboplatin, doxorubicin, and paclitaxel
P4	66	Papillary cancer, recurrent ascites	Carboplatin, paclitaxel, doxorubicin liposomal, gemcitabine, and topotecan
P5	85	Ovarian cancer, new ascites	Carboplatin, and paclitaxel
P6	60	Cervical cancer and recurrent ascites	Cisplatin, carboplatin, and paclitaxel

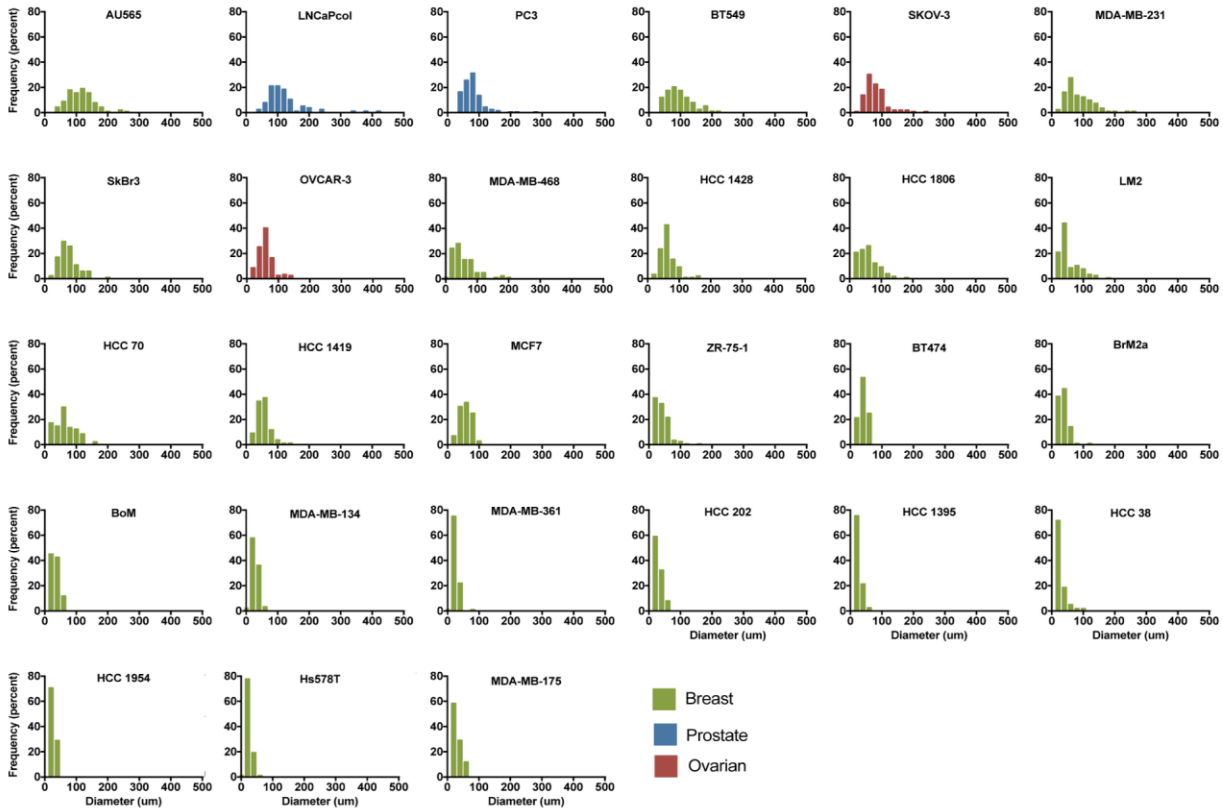

Figure S1. MCTS size distribution in polyNIPAAM.
Histograms of Day 14 diameters for MCTS formed in polyNIPAAM. Cell lines are ordered from the highest to the lowest mean diameter across 23 breast (green), 2 prostate (blue), and 2 ovarian (red) cancer cell lines.

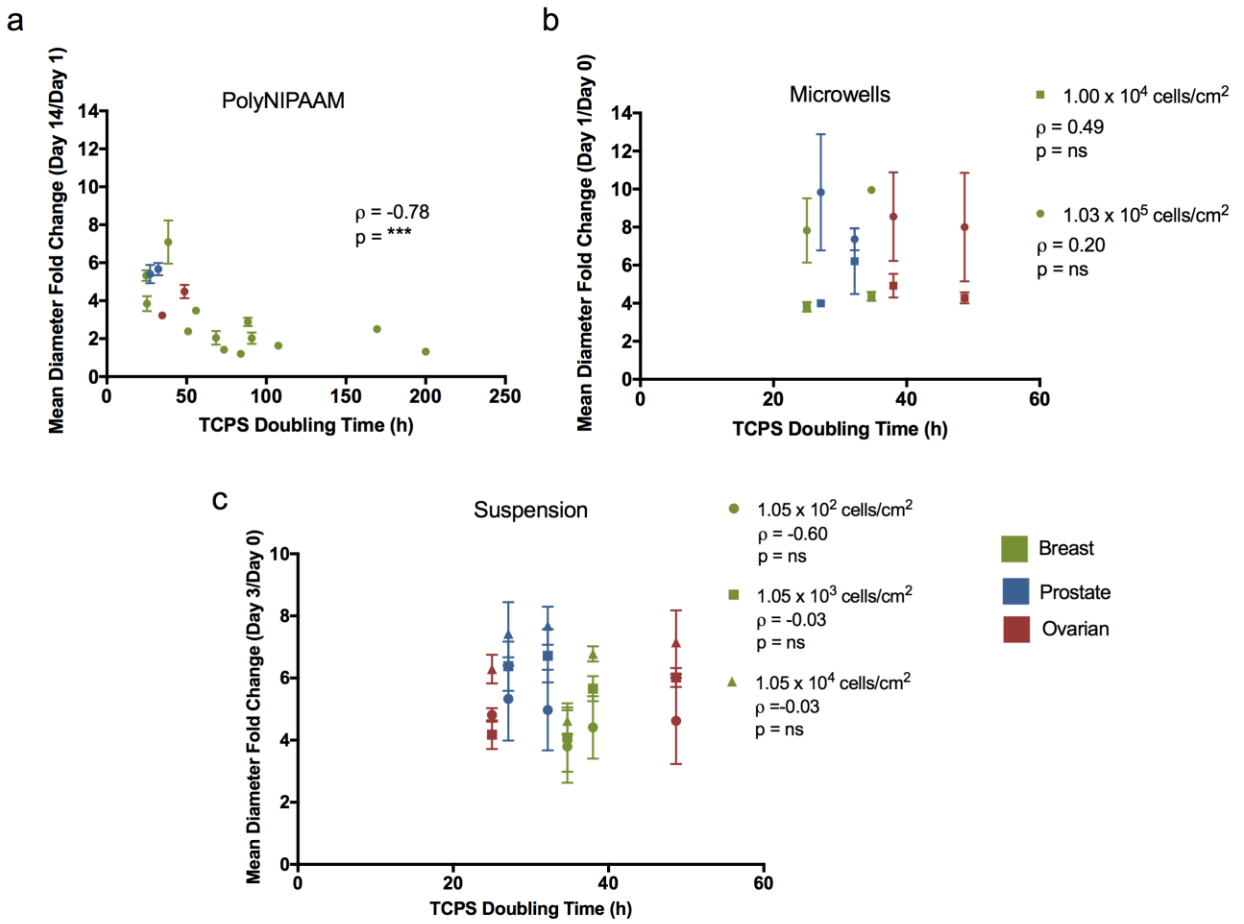

Figure S2. PolyNIPAAM MCTS size negatively correlated with TCPS doubling time.
a. Mean diameter fold change in polyNIPAAM vs. TCPS doubling time. b. Mean diameter fold change in microwells vs. TCPS doubling time. c. Mean diameter fold change in suspension vs. TCPS doubling time. Data for 13 breast (green), 2 prostate (blue), and 2 ovarian (red) cancer cell lines are shown. Mean diameter fold change measures how MCTS diameters changed from Day 1 to Day 14. Spearman rank correlation is reported as ρ with significance (p) determined by a two-tailed t-test. Doubling times are from Heiser, *et al*[46].

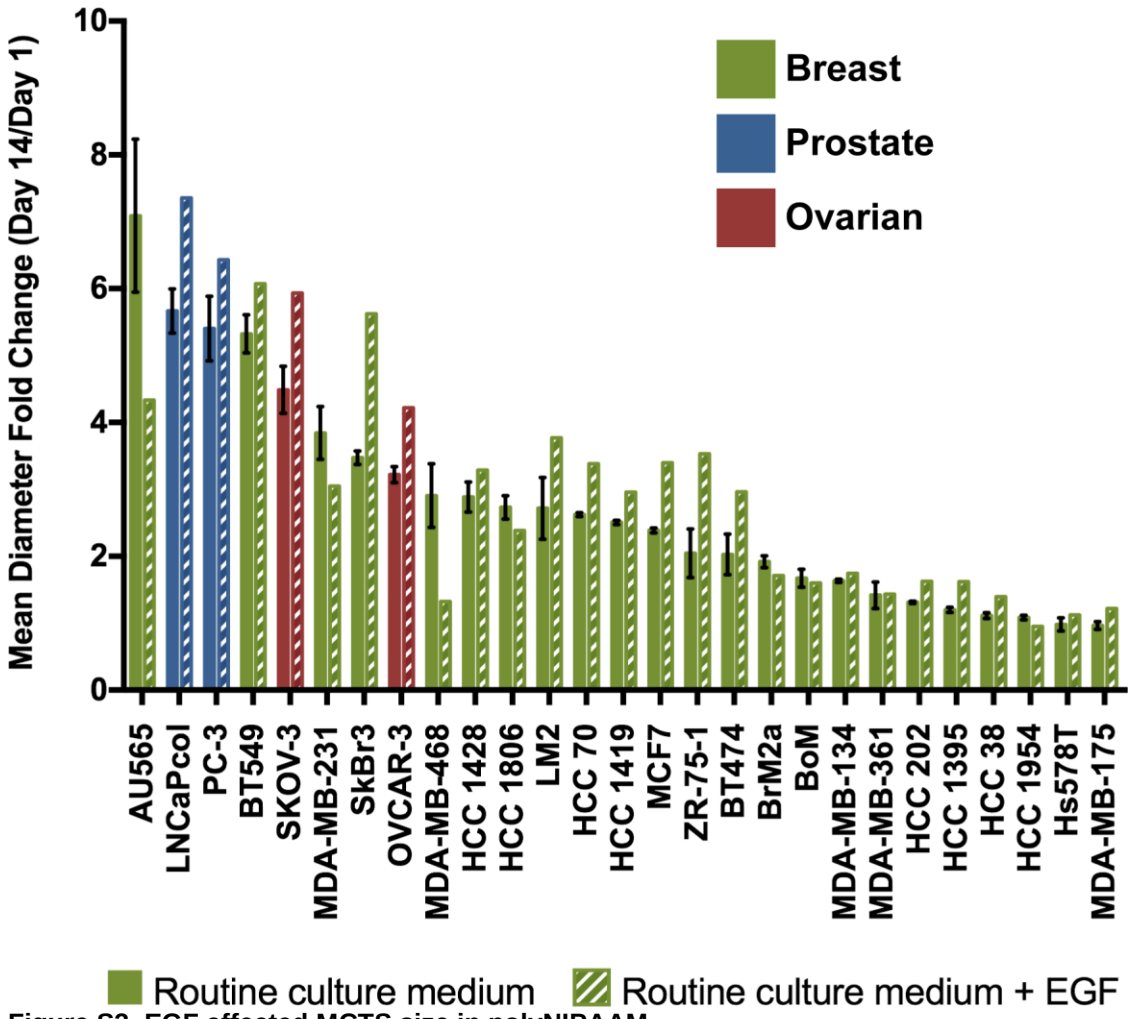

Figure S3. EGF affected MCTS size in polyNIPAAM.
Mean diameter fold change in polyNIPAAM of 23 breast (green), 2 prostate (blue), and 2 ovarian (red) cancer cell lines seeded with routine culture medium (solid bars) or routine culture medium + EGF (pattern bars). Mean diameter fold change measures how MCTS diameters changed from Day 1 to Day 14.

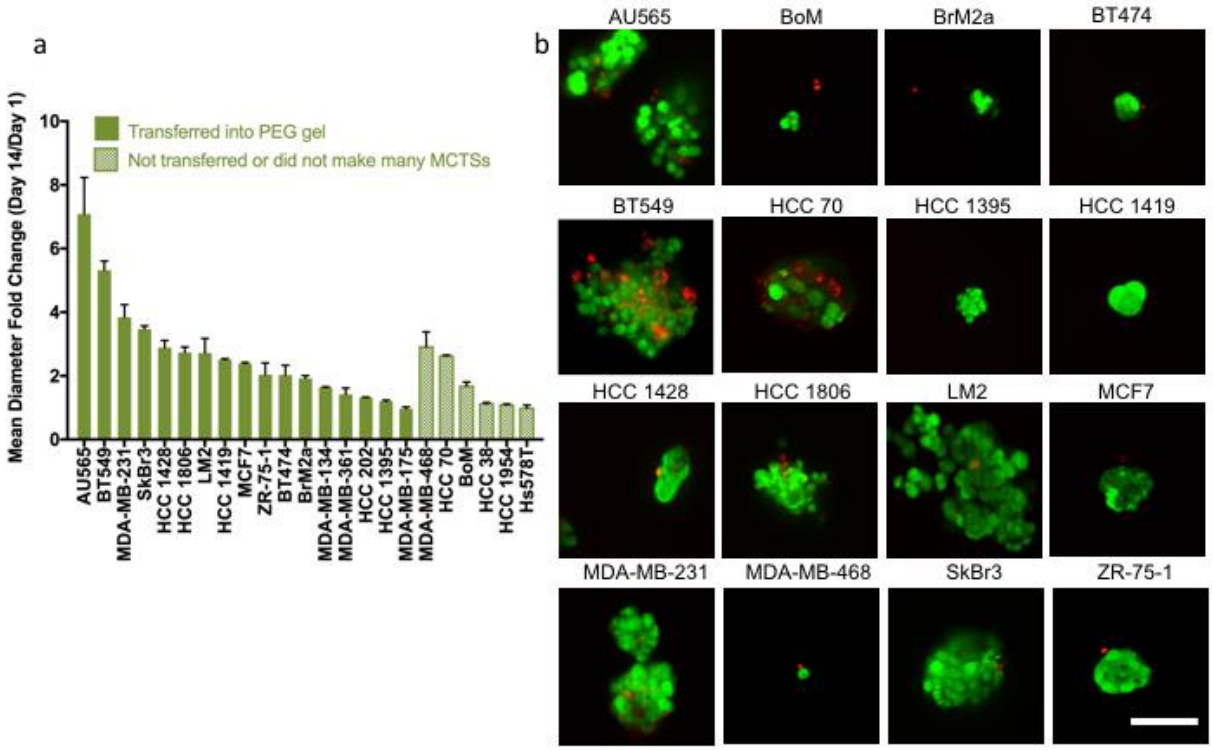

Figure S4. Many breast cancer cell lines formed MCTS in polyNIPAAM and could be transferred to 3D PEG-MAL hydrogel.

a. Mean diameter fold change of 23 breast cancer cell lines grown into MCTS in polyNIPAAM. Mean diameter fold change measures how MCTS diameters changed from Day 1 to Day 14. b. Live/dead images of MCTS (green: live cells, red: dead cells) in PEG-MAL hydrogels. Images taken 3 days post-encapsulation. Scale bar: 100 μm.

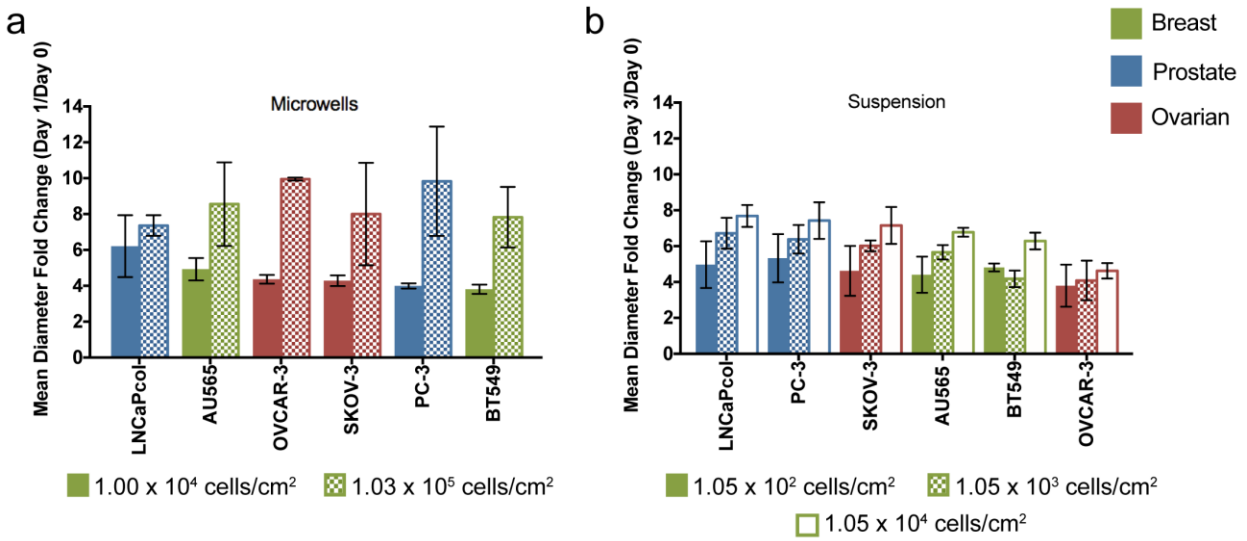

Figure S5. MCTS size increased with seeding cell density in microwells and suspension.
a. Effect of cell density on MCTS size in microwells (low density: $1.00x10^4$ cells/cm^2-solid bars and high density: $1.03x10^5$ cells/cm^2-pattern bars). b. Effect of cell density on MCTS size in suspension (low density: $1.05x10^2$ cells/cm^2-solid bars, medium density: $1.05x10^3$ cells/cm^2-pattern bars, and high density: $1.05x10^4$ cells/cm^2-empty bars). Data for 2 breast (green), 2 prostate (blue), and 2 ovarian (red) cancer cell lines are shown. ANOVA with the Tukey post-test was applied to individual cell lines for each method. No statistically significant differences between seeding densities were observed in any cell line-method combination.

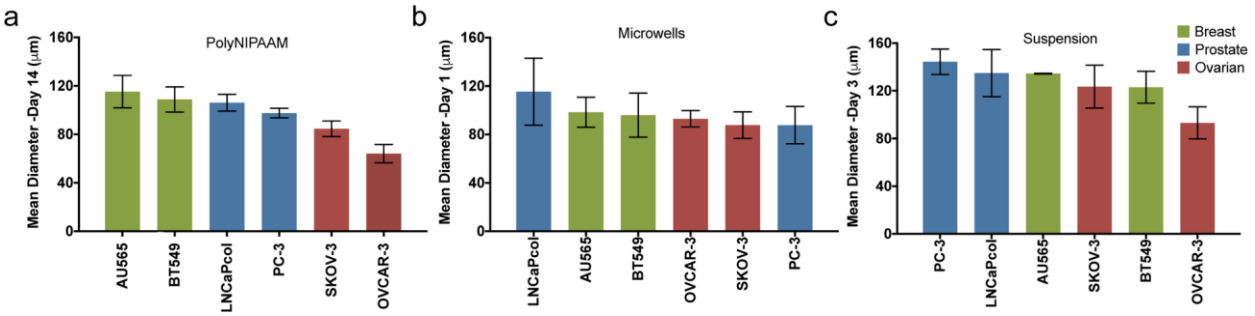

Figure S6. MCTS reached sizes around 50-150 µm.

a. Mean diameter in polyNIPAAM at day 14 (density: 100 cells/µL). b. Mean diameter in microwells at day 1 (density: 1.00×10^4 cells/cm^2). c. Mean diameter in suspension at day 3 (density: 1.05×10^4 cells/cm^2). Data for 2 breast (green), 2 prostate (blue), and 2 ovarian (red) cancer cell lines are shown. ANOVA with Tukey post-test was used to compare statistically significant differences across methods for each cell line: PC-3 (polyNIPAAM vs. suspension**) and (microwells vs. suspension*).

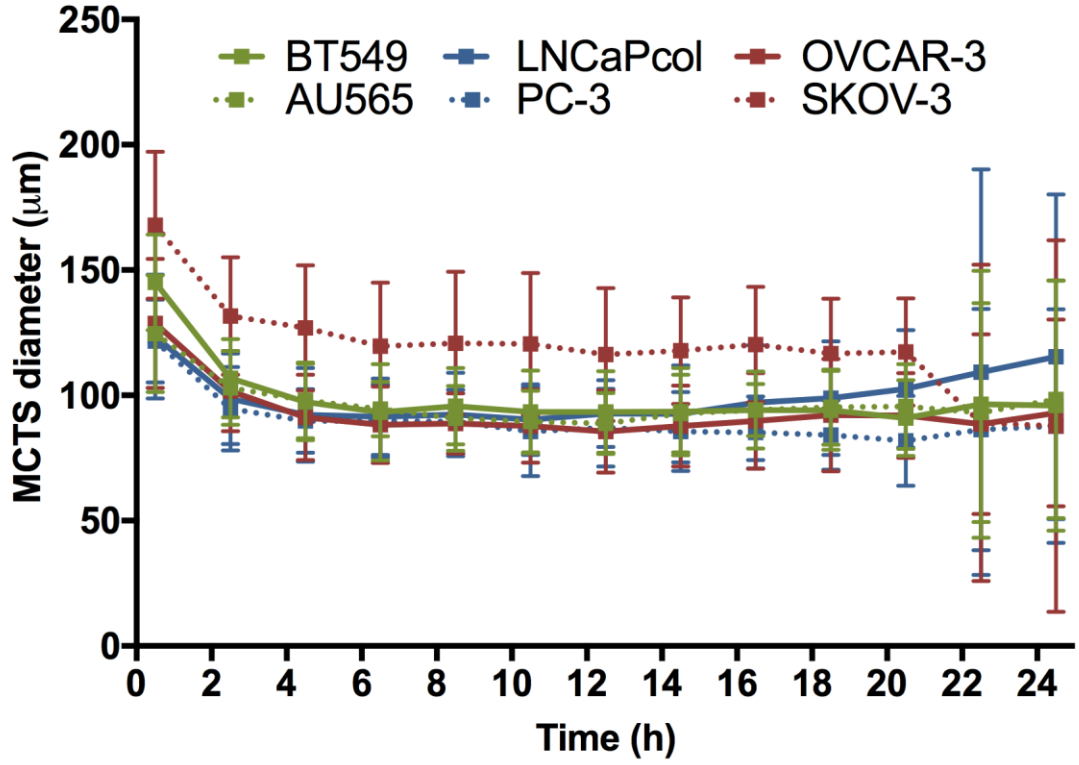

Figure S7. MCTS became compact over time in microwells.
MCTS diameter over time of 2 breast (AU565 and BT549, green), 2 prostate (LNCaPcol and PC-3, blue), and 2 ovarian (OVCAR-3 and SKOV-3, red) cancer cell lines for 24 hours after seeding in microwells.

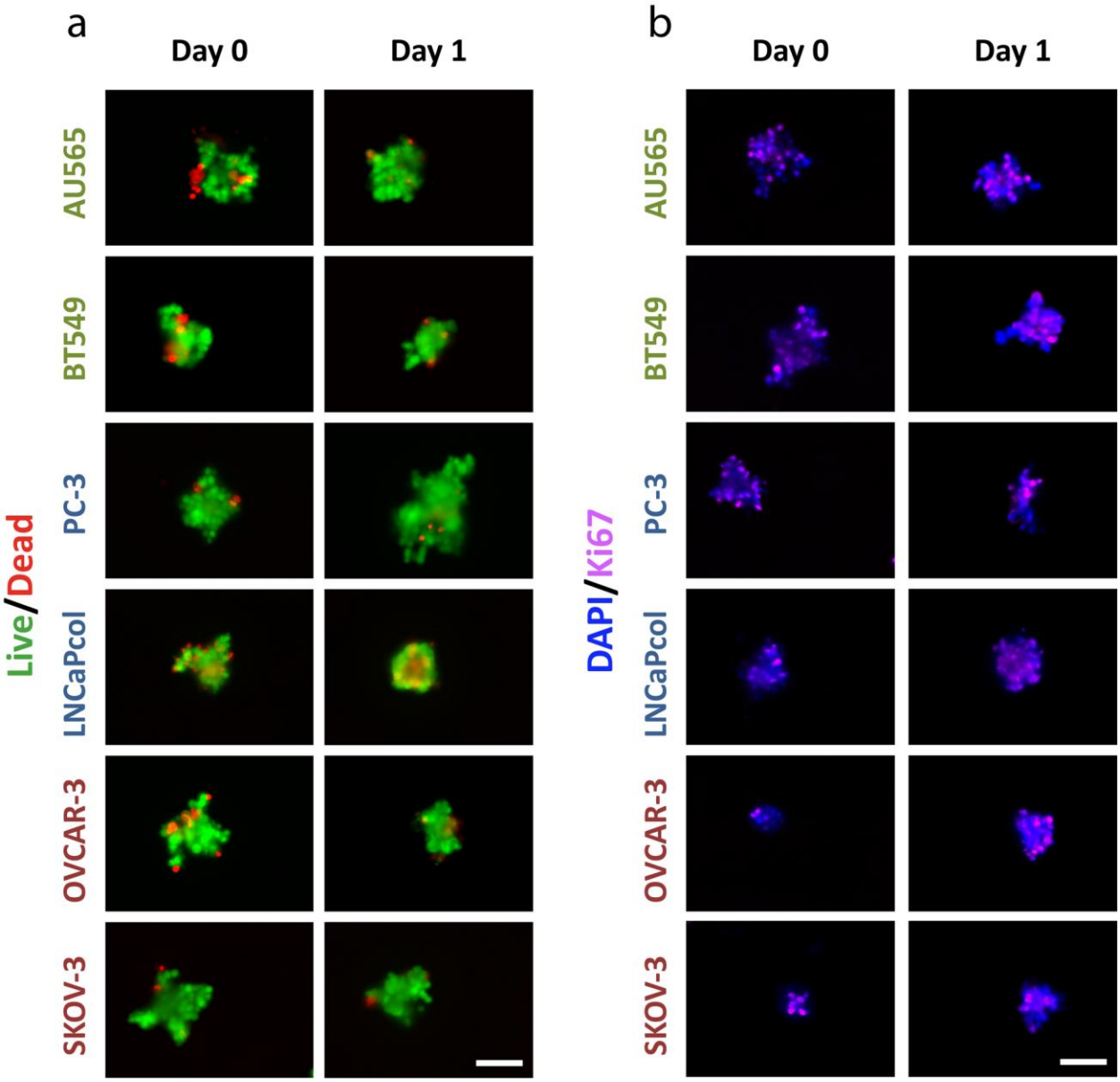

Figure S8. MCTS proliferated in microwells.
a. Live/dead staining of MCTS (green: live cells, red: dead cells). Scale bar: 100 μm. b. Ki67 staining of MCTS (purple: Ki67, blue: DAPI). Images for 2 breast (green), 2 prostate (blue), and 2 ovarian (red) cancer cell lines are shown. Scale bar: 100 μm.

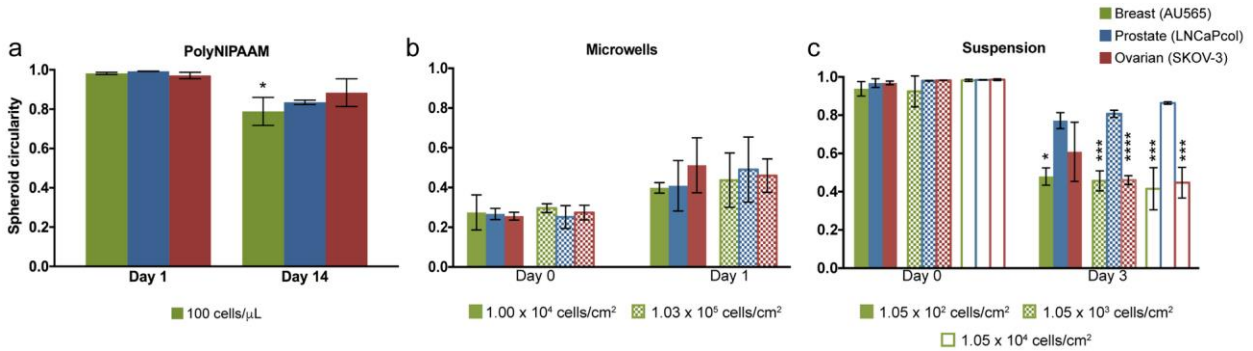

Figure S9. Circularity was preserved in polyNIPAAM, increased in microwells, and decreased in suspension.

a. MCTS circularity in polyNIPAAM (from Day 1 to Day 14). b. MCTS circularity in microwells (from Day 0 to Day 1). Low density: $1.00x10^4$ cells/cm^2-solid bars, and high density: $1.03x10^5$ cells/cm^2-pattern bars. c. MCTS circularity in suspension (from Day 0 to Day 3). Low density: $1.05x10^2$ cells/cm^2-solid bars, medium density: $1.05x10^3$ cells/cm^2-pattern bars, and high density: $1.05x10^4$ cells/cm^2-empty bars. AU565 breast (green), LNCapcol prostate (blue), and SKOV-3 (red) cancer cell lines. Within each method, ANOVA followed by Tukey post-test was applied to individual cell lines separately for each seeding density. Cell line-seeding density combinations with a statistically significant difference between initial and final values are marked.

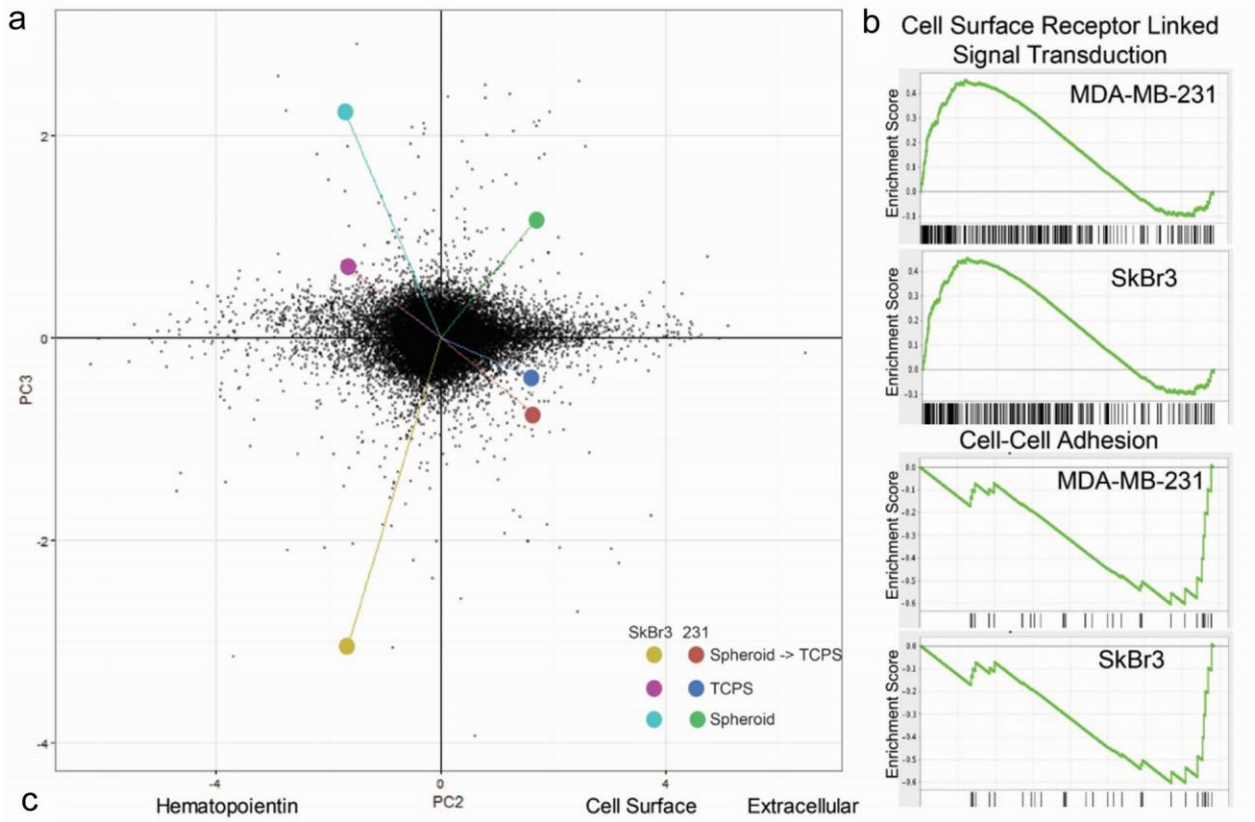

c

	Hematopoientin Interferon Domain Cytokine Receptor Binding	Regulation of Growth	Response to Wounding	Cell Surface Receptor Linked Signal Transduction	Extracellular Structure Organization and Biogenesis	Cell-Cell Adhesion	Detection of Stimulus	Peptidase Activity
SkBr3	1.91	1.84	1.72	1.69	1.62	-1.62	-1.36	-1.28
MDA-MB-231	1.85	1.84	1.73	1.68	1.62	-1.63	-1.32	-1.29

Figure S10. RNA-Seq on breast cancer cells revealed enrichment of surface receptor linked signal transduction.

a. Principal component analysis of MDA-MB-231 and SkBr3 grown on TCPS, in polyNIPAAM for 14 days, or grown in polyNIPAAM and then dissociated and plated back onto TCPS. b. Gene set enrichment analysis showed that cell surface receptor linked signal transduction was enriched on TCPS over MCTS, and cell-cell adhesion was enriched in MCTS as compared to TCPS, for MDA-MB-231 and SkBr3 cells. c. Several gene set categories were significantly enriched on TCPS (positive values) or in MCTS in 3D (negative values).

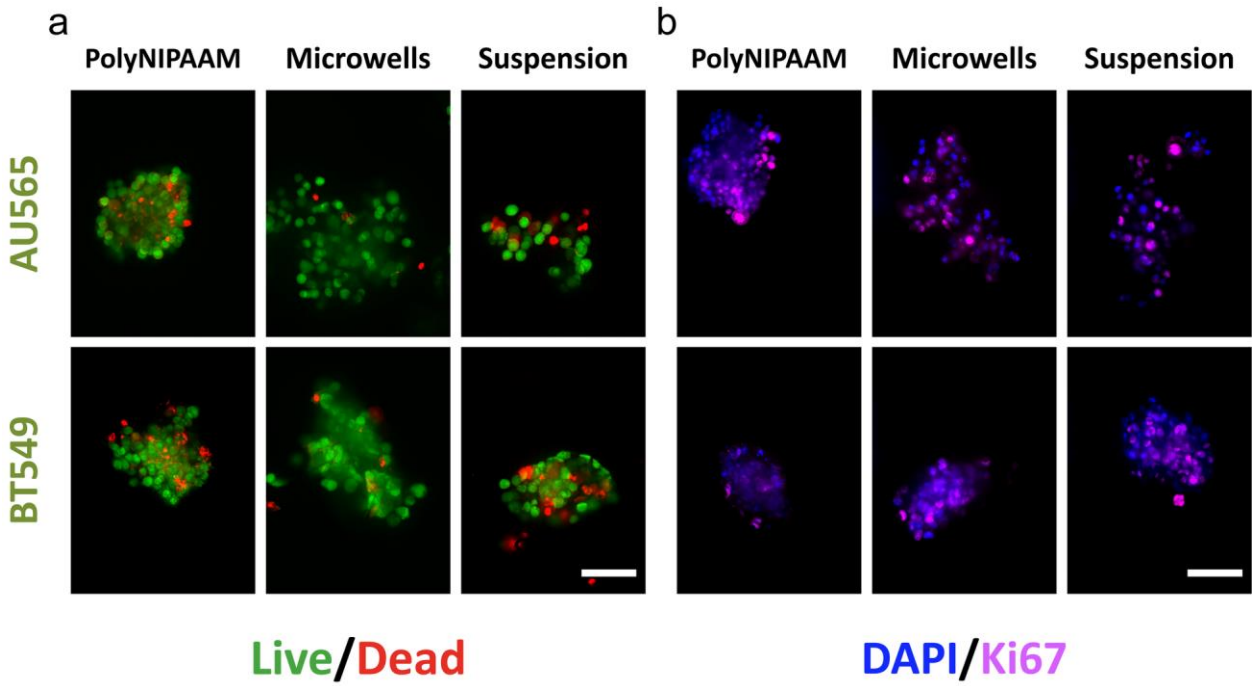

Figure S11. MCTS formed in polyNIPAAM, microwells, and suspension could be encapsulated in PEG-MAL.

a. Live/dead staining of MCTS (green: live cells, red: dead cells) encapsulated in 10 wt% PEG-MAL hydrogels with cell adhesion peptide RGD. b. Ki67 staining of MCTS (purple: Ki67, blue: DAPI) encapsulated in 10 wt% PEG-MAL hydrogels with cell adhesion peptide RGD. Images for breast cancer (AU565 and BT549) cell lines are shown. Scale bar: 100 μm.